3-D Position Sensitive CdZnTe Spectrometer Performance Using Third Generation VAS/TAT Readout Electronics

Feng Zhang, Zhong He, *Senior Member, IEEE*, Glenn F. Knoll, *Fellow, IEEE*, David K. Wehe, *Senior Member, IEEE*, and James E. Berry

***Abstract*—Three-dimensional (3-D) position-sensitive CdZnTe (CZT) gamma-ray spectrometers employing new VAS3.1/TAT3 ASIC readouts were developed and tested. Each spectrometer is a $1.5 \times 1.5 \times 1$ cm^3 CdZnTe crystal with 11×11 pixellated anodes wire-bonded to the readout electronics using an intermediate ceramic substrate with plated-through-via. The signals from the anode pixels and the cathode were all read out using these ASICs. The pixel position provides the lateral coordinates of interactions, while the cathode to anode signal ratio and electron drift times are used to obtain interaction depths. Using the 3-D position information, the variation in weighting potential, electron trapping and material nonuniformity can be accounted for to the scale of the position resolution, $\sim 1.27 \times 1.27 \times 0.2$ mm. The new VAS3.1/TAT3 ASIC has less gain and baseline drift, lower cross-talk noise, more uniform thresholds, better linearity and better timing resolution than our previous VAS2/TAT2 system. For example, the 32 keV K X-ray from a ^{137}Cs source was observed for the first time. Two 3-D position sensitive CZT spectrometers were tested and both achieved better than 1% FWHM energy resolution (at 662 keV, room temperature operation, with an uncollimated source) for single-pixel events. The experimental results for these two 3-D position sensitive CZT spectrometer systems are presented and discussed.**

***Index Terms*—CdZnTe, CZT, gamma-ray spectroscopy, position sensitive, spectrometer, three-dimensional (3-D).**

I. Introduction

WIDE band gap semiconductor detector materials, such as CdTe, CdZnTe and HgI_2, have long been of interest because of the convenience of room temperature operation, high efficiency for gamma-ray detection and potential for good energy resolution. Among them, CdZnTe has gained particular interest. However, the performance degradation due to charge trapping limits its application using conventional planar electrodes when large sensitive volumes are needed. Single polarity charge sensing techniques, such as coplanar grids [1] or pixellated anodes [2], can overcome the severe hole trapping problem and greatly improved the energy resolution of large volume CdZnTe detectors. However, even with single polarity charge sensing techniques and methods to compensate for electron trapping, such as relative gain [1] and depth sensing [3], the variations in electron trapping and material nonuniformity can still degrade the energy resolution on a coplanar-grid detector.

In 1998, we developed the first fully functional three-dimensional (3-D) position sensitive CZT spectrometer [4], [5]. The 3-D position sensitivity of this CZT spectrometer using VA1 application specific integrated circuits (ASIC) chips enabled the correction for material nonuniformity and varying electron trapping. An energy resolution of 1.7% FWHM at 662 keV was achieved for single-pixel events from the whole bulk of a 1 cm^3 3-D position sensitive CZT detector. However, this first-generation 3-D position sensitive CZT spectrometer could only record the energy and 3-D position information for single-pixel events.

After five years of effort and a fruitful collaboration between our group and Ideas ASA [6], in 2003 we introduced the second-generation 3-D position sensitive CZT system using the VAS2/TAT2 ASIC [7]. With the ability of sensing the electron drift time for each individual interaction, these second-generation 3-D position sensitive CZT systems can measure the energy depositions and 3-D position coordinates for multiple-pixel events, as well as single-pixel events. Intelligent gamma-ray spectroscopy [8] and 4π Compton imaging [9] have been successfully implemented using these second-generation 3-D position sensitive CZT spectrometers.

Several problems were discovered in the second-generation readout electronics. First, the electronic noise was fairly high ($\sim$5–6 keV in different channels), limiting the energy resolution to 1.1% FWHM at 662 keV for single-pixel events. Second, some design flaws on the front-end board caused substantial cross-talk noise on the cathode signal induced by digital control signals. This led to a high cathode triggering threshold ($\sim$100 keV). Third, only one global threshold could be set for all the channels reading signals from anode pixels. Because of the variations of dc offsets on these channels, the global threshold had to be set above the highest threshold of all channels, causing a fairly high triggering threshold for the anode pixels ($\sim$80 keV). Last, significant nonlinearity was observed in the VAS2 (energy) channels, increasing the complexity in the calibration and degrading the energy resolution for multiple-pixel events. As a result, the best energy resolution achieved was 1.6% FWHM for two-pixel events and 2.1% FWHM for three-pixel events.

The third-generation ASIC-VAS3.1/TAT3 has been designed to address the problems described above. This paper briefly introduces the basic system configuration of the third-generation

Manuscript received November 13, 2004. This work was supported by the DOE/NNSA NA-22 office under Grant DE-FG03-01NN20122.

The authors are with the Department of Nuclear Engineering and Radiological Sciences, University of Michigan, Ann Arbor, MI 48109 USA (e-mail: zhangf@umich.edu).

Digital Object Identifier 10.1109/TNS.2005.856821

3-D position sensitive CZT spectrometers. The experimental results from two detector systems are presented and discussed.

II. System Description

A 3-D position sensitive CZT spectrometer consists of a CdZnTe detector module with a ceramic substrate, an ASIC front-end board, and a controller (repeater) card (MCR3). The CdZnTe detector is wire-bonded to the ASIC inputs using an intermediate ceramic substrate with plated-through-via. The MCR3 repeater card is used to generate and send the readout clock signals to the ASIC and also convert the output of the ASIC from current to the voltage signals needed at the input of the data acquisition (DAQ) board. A PCI-6110 DAQ board from National Instruments is used as the A/D converter and as the controller interface between the DAQ program and the detector system.

A. Pixellated CdZnTe Detector and Front-End Board

Both detectors were fabricated by eV-Products [10] in 2001. Each has an 11×11 pixellated anode and a planar cathode on a $1.5 \times 1.5 \times 1.0$ cm^3 CZT crystal. The pixel pitch is 1.27 mm. There is a common grid between pixel anodes biased at negative voltage to focus the electrons to pixel anodes. The trace width of the grid electrode is 100 μm with a 200 μm gap between the grid and pixel anodes.

Four 33-channel VAS3.1/TAT3 chipsets are mounted on the front-end board to read out signals from 121 anode pixels and the cathode. The CZT crystal is mounted on a ceramic plate. The conducting traces on the two sides of the ceramic plate connect every pixel anode to a corresponding metal pad on the periphery of the plate. A short wire-bond connects each pad on the ceramic plate to the input of each ASIC channel on the front-end board, as shown in Fig. 1.

B. ASIC

The basic structure of the VAS3.1/TAT3 ASIC is nearly the same as the VAS2/TAT2 ASIC [7]. Several changes aiming to improve the system performance have been implemented in the VAS3.1/TAT3 ASIC. In the VAS2, because one channel (special channel) was used to read out the cathode signal (positive pulse) and the other channels (normal channels) were used to read out anode signals (negative pulse), an inverter was added after the shaper in each normal channel to make the polarity of anode signals the same as the cathode polarity, so that all channels could employ a common peak-hold circuitry. However, the inverter is highly sensitive to temperature variation, causing a drifting of the baseline and the gain. This problem was solved with the use of two peak-hold circuits, one for anode signals and the other for the cathode signal, and the removal of the inverter. Other changes include adding a test channel with the peak hold turned off, using separate controls for the preamp feedback resistance for the special channel and the normal channels, and increasing the gain on TAT3 chips, all of which help to diagnose the system response and improve the system performance.

The VAS3.1 (version 3.1) ASIC chip is used to read out the induced charges on the anode pixels and the cathode. The TAT3 (version 3) ASIC chip is used to trigger the system and read out

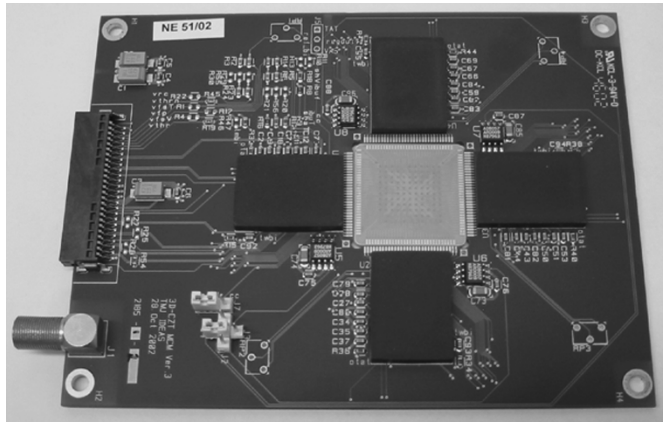

Fig. 1. ASIC front-end board with the CdZnTe detector placed in the center and wire-bonded to the ASIC inputs.

electron drift times. One VAS3.1 chip and one TAT3 chip form a chipset. The preamplifier output of each VAS3.1 channel is wire-bonded to the input of each TAT3 channel.

Each VAS3.1 chip has 33 independent channels, each consisting of a preamplifier, a shaping amplifier, a peak-hold and sample-hold circuitry. The first channel on each VAS3.1 chip has an opposite polarity to the other 32 channels, to read out the cathode signal. Fig. 2 shows the basic structure of a single VAS3.1/TAT3 channel.

Each TAT3 chip also has 33 channels, each channel having a fast shaper, a discriminator for triggering and a time-to-amplitude converter (TAC) for measuring the electron drift time. A trigger mask can be set to disable those channels having high noise.

C. Depth Sensing Using C/A Ratio and Electron Drift Time

In a 3-D position sensitive CZT spectrometer, the 2-D coordinates of interactions are determined from the individual location of the triggering pixels. For single-interaction events, because of the shape of the weighting potential, the cathode signal is proportional to both the deposited energy and the interaction depth, while the anode signal is nearly proportional only to the deposited energy. Thus, the interaction depth can be derived from the cathode to anode signal ratio [3]. However, for multiple-interaction events, we cannot obtain the depth for each individual interaction using this signal ratio. Instead, electron drift times for each triggering pixel are individually recorded. Assuming nearly constant electron drift velocity inside the detector volume, the electron drift time can be used to obtain the depth for multiple-pixel events [7].

Fig. 3 illustrates the timing sequences of the electron drift-time measurements for multiple-pixel events. When a gamma ray interacts in the detector and the electron clouds start to drift, a trigger is generated by the TAT3 special channel when the induced signal on the cathode crosses a threshold. This trigger starts the TAC in the TAT3 special channel and generates the system trigger. When an electron cloud approaches close to an anode pixel, the induced signal crosses a threshold, and triggers the corresponding TAT3 channel. This trigger starts the TAC in the TAT3 channel corresponding to that anode pixel. After a fixed delay (2–3 μs) following the system trigger, all

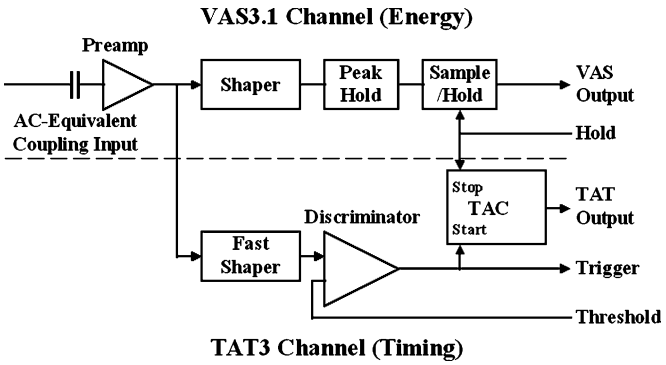

Fig. 2. Illustration for the VAS3.1 (energy) and the TAT3 (timing) channels.

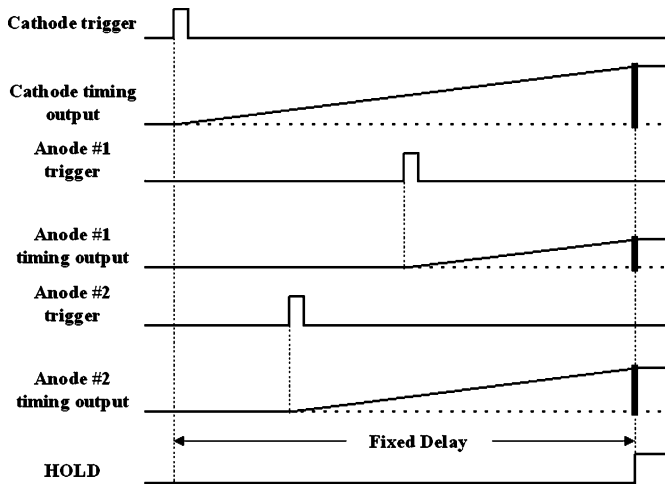

Fig. 3. Interaction depth determination by electron drift time sensing.

channels are held by sample-hold circuits, and read out in serial mode through a multiplexer built into the chips. By using peak-hold in addition to sample-hold circuits on the VAS ASIC, the pulse amplitude of multiple-pixel events with different electron drift times (different peaking times) due to different interaction depths can be obtained correctly. The individual electron cloud drift times can be derived from the timing signal amplitudes generated by the TACs in the TAT3 channels.

D. DAC Thresholds

In the second-generation system, the anode pixels had triggering thresholds ranging from 50 to 80 keV, with the spread caused by the variations of dc offsets and noise in each ASIC channel. However, only one global triggering threshold could be set for all channels reading the anode pixels. As a result, the threshold needed to be set above the highest threshold among all channels ($\sim$80 keV). This problem has been solved in the new TAT3 ASIC. In addition to the global threshold, a 4-bit digital-to-analog converter (DAC) unit has been added to each TAT3 channel so that the threshold of each channel can be finely tuned to achieve more uniform and lower thresholds among all the channels.

III. Experimental Results

Two 3-D position sensitive CZT detector systems were assembled and tested with the third-generation readout electronics. The first detector was biased at -2200 V on the cathode and the second at -1400 V. The anode pixels were dc-coupled to the ASIC inputs and thus all were at ground potential. The common grid electrode between the pixels was biased at a negative voltage to steer electrons drifting toward the anode pixels.

The whole system was operated at room temperature $\sim$ 23 °C. The detector was irradiated from the cathode side with uncollimated gamma-ray sources placed 5 cm away from the cathode. Data collected from a ^{137}Cs gamma-ray source was used for the calibration. Spectra from a ^{241}Am source were also collected for measuring the electron mobility-lifetime products and estimating the electronic noise.

A. Improvements With the New Electronics

One problem of the second-generation 3-D position sensitive CZT system was that the baseline and the gain of the VAS2 ASIC were both very sensitive to temperature changes. Although the baseline drift can be dynamically monitored and compensated by a specially designed DAQ program, and the gain drift can be calibrated for a range of environmental temperatures, these temperature dependences still complicate the system calibration and degrade energy resolution. This problem has been solved on the new VAS3.1 ASIC [11]. Both the baseline and the gain were fairly stable in the third-generation 3-D position sensitive CZT system when the temperature varied by a few degrees Celsius during the 40 h of data collection.

Another limiting factor on the performance of the second-generation system was the large cross-talk induced on the cathode due to the improper layout (differential digital signal traces not in parallel) of the digital signal traces on the front-end board. As a consequence, the triggering threshold of the cathode signal had to be set above 100 keV to prevent the system from being retriggered continuously by the cross-talk. Since the anode pixels have much smaller area than the cathode, the induced cross-talk on the anode pixels was not as large but was still not negligible. The triggering threshold of the anode signal ranged from 50 to 80 keV, varying from channel to channel due to the variations in dc offsets. Due to the newly designed front-end board of the third-generation system, the cross-talk noise, although still present, has been greatly reduced. As a result, the cathode triggering threshold has been lowered to $\sim$50 keV and the anode triggering threshold has been lowered to $\sim$25–35 keV.

B. Electronic Noise

According to the test report from Ideas ASA, the electronic noise in the ASIC is $\sim$3 keV FWHM. However, due to a design limitation, the electronic noise of the ASIC cannot be directly measured after the ASIC and the detector are connected. In order to estimate the overall electronic noise of the system, an uncollimated ^{241}Am source was placed 5 cm away from the cathode. Nearly 75% of the 59.5 keV gamma rays from the ^{241}Am source should be stopped in the first 0.5 mm thin layer on the cathode side. Thus, most of the collected anode signals should come from interactions at almost the same depth, with

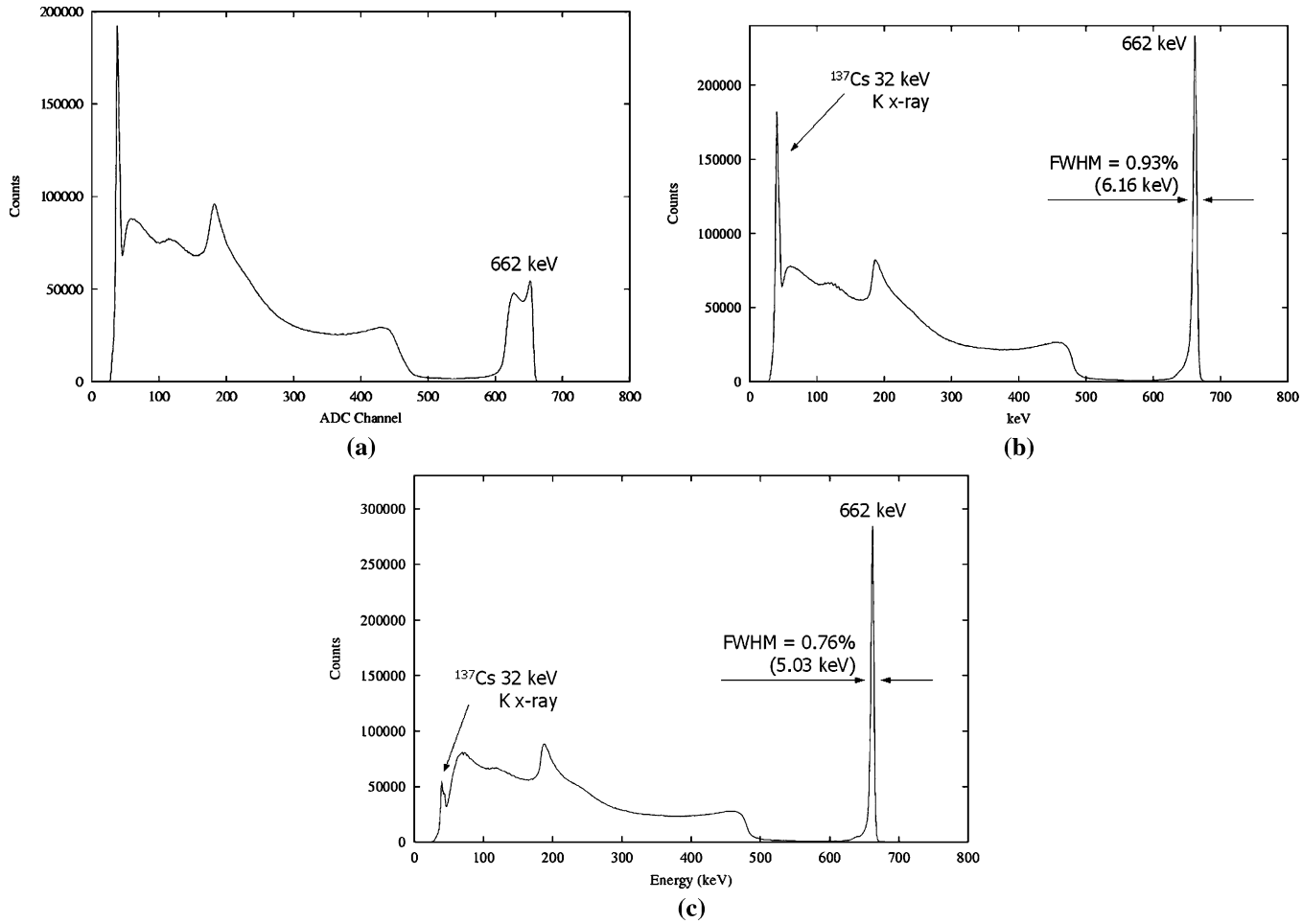

Fig. 4. Energy spectra of single-pixel events from an uncollimated ^{137}Cs source collected for 40 h from all working pixels. The events triggered by only the anode signal are included in order to show the low energy K X-ray. (a) Raw spectrum of detector #1 before 3-D correction (ASIC gain variation corrected). (b) Energy spectrum of detector #1 after 3-D correction. The detector was biased at -2200 V on the cathode and -65 V on the grid). (c) Energy spectrum of detector #2 after 3-D correction. The detector was biased at -1400 V on the cathode and -45 V on the grid.

only very small broadening due to depth dependence. The energy resolution of the ^{241}Am anode spectrum was measured to be $\sim$4.8 keV FWHM. The statistical fluctuation in the charge carrier creation assuming a Fano factor of 0.1 can be subtracted, leaving the electronic noise of the channels reading out anode signals estimated at less than 4.5 keV FWHM. Similarly, the electronic noise in the channel reading out the cathode signal was estimated to be $\sim$7 keV FWHM.

C. Results for 662 keV Single-Pixel Events

Before the 3-D calibration of the detector response [7], [12], the raw energy spectrum of a ^{137}Cs source had a broadened 662 keV photopeak due to the variations in the detector response under different pixels and at different depths, as can be seen in Fig. 4(a). With the help of 3-D position sensing, the material nonuniformity, the weighting potential variations and the electron trapping variations can be accommodated to the limit of the position resolution—estimated to be $1.27 \times 1.27 \times 0.2$ mm. By implementing 3-D calibration and correction, remarkable energy resolutions of 0.93% and 0.76% FWHM at 662 keV for single-pixel events have been achieved from the entire 2.25 cm^3 volumes the detectors [cf. Fig. 4(b) and (c)]. As a result of the much lower thresholds than the previous systems, the 32 keV ^{137}Cs K X-rays have been observed in both systems for the first time. The much smaller 32 keV photopeak in Fig. 4(c) is due to the higher thresholds in the second system.

Fig. 5 shows the distributions of energy resolution (FWHM at 662 keV) across the detector surface for the two devices for single-pixel events. The two bad pixels are probably due to faulty wire-bonds. The first detector has 88 of 121 pixels that have better than 1% FWHM energy resolution, while the second detector has 116 pixels with better than 1% FWHM energy resolution.

D. Measurements of $(\mu\tau)_e$

The energy spectra of an ^{241}Am source irradiating the cathode side were collected for each pixel under two different cathode biases (-1400 and -2200 V for the first detector, -1400 and -2000 V for the second detector). The electron mobility lifetime product can be estimated using [13]

$$(\mu\tau)_e = \frac{D^2}{\ln\left(\frac{H_{a1}}{H_{a2}}\right)}\left(\frac{1}{V_2} - \frac{1}{V_1}\right) \tag{1}$$

where D is the detector thickness, H_{a1} and H_{a2} are the photopeak centroids under two different cathode biases—V_1 and V_2. The measured $(\mu\tau)_e$ for all the pixels are shown in Fig. 6. The

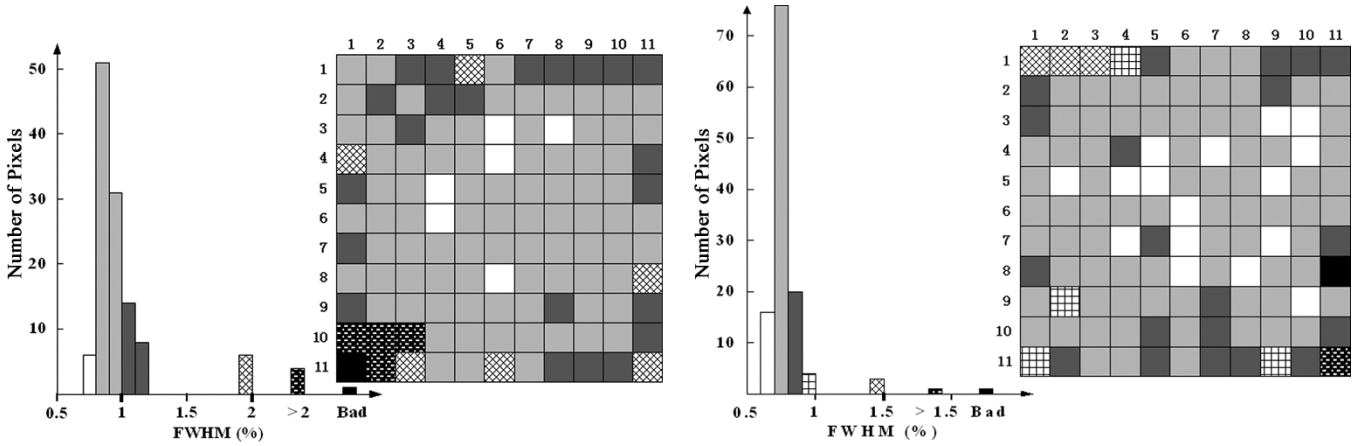

Fig. 5. Energy resolution distribution for single-pixel events from a uncollimated ^{137}Cs source collected over 40 h for (a) detector #1, biased at −2200 V on the cathode and −65 V on the grid. (b) Detector #2, biased at −1400 V on the cathode and −45 V on the grid.

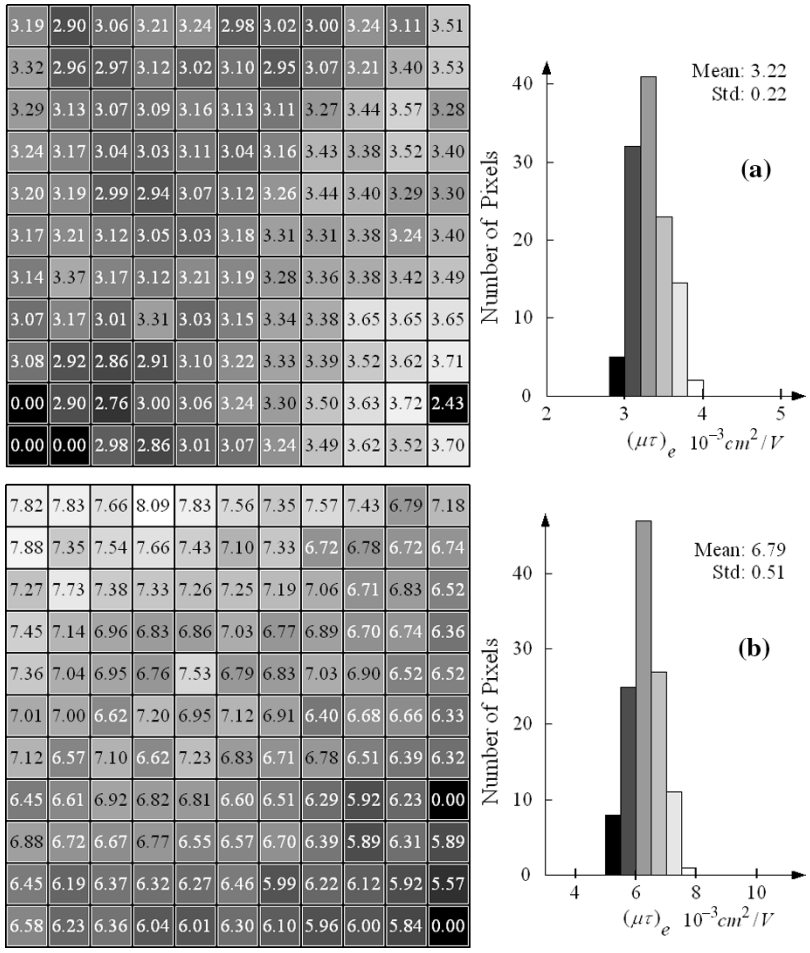

Fig. 6. $(\mu\tau)_e$ distribution for single-pixel events from a ^{137}Cs source collected over 40 h for (a) detector #1. (b) Detector #2.

error in the $(\mu\tau)_e$ measurements should be mainly due to the error in the depth measurements (∼1%), as discussed in [13]. We can see that the mean $(\mu\tau)_e$ of the second detector is more than two times that of the first detector. This might be the reason why the second detector achieved much better energy resolution than the first. The pixels with zero $(\mu\tau)_e$ are bad or poor pixels that do not have sufficient data to calculate the $(\mu\tau)_e$.

E. Results for 662 keV Multiple-Pixel Events

For multiple-pixel events, the depth of each interaction can be derived from the electron drift time for each pixel. After correction for timing-amplitude-walk, electron trapping and nonlinearity for each signal, the true energy and 3-D position information can be obtained for each interaction.

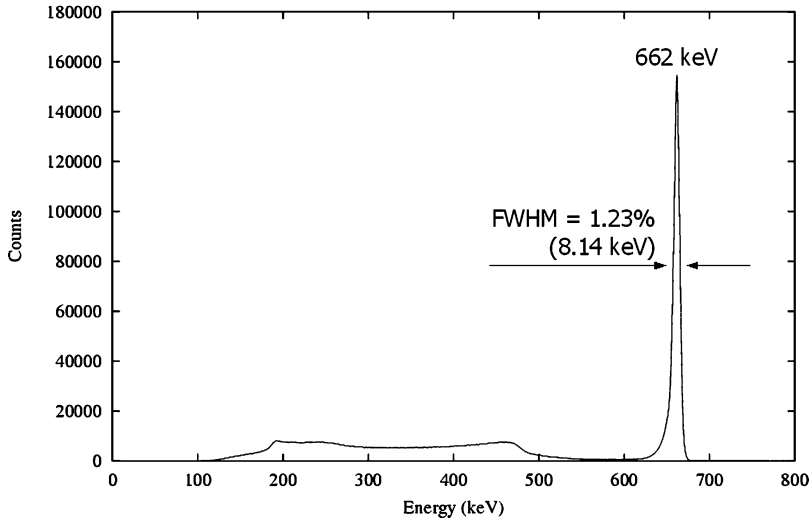

Fig. 7. Energy spectrum of two-pixel events from an uncollimated ^{137}Cs source collected for 40 h from the whole volume of detector #2. The detector was biased at −1400 V on the cathode and −45 V on the anode grid.

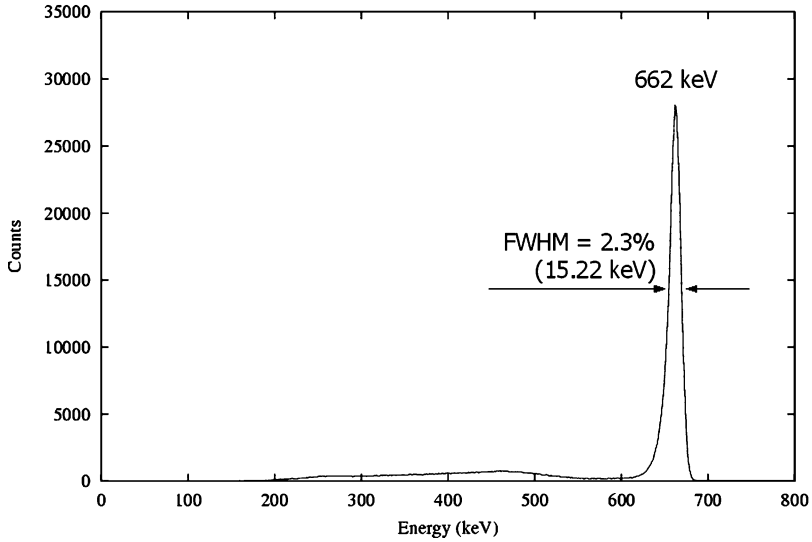

Fig. 8. Energy spectrum of three-pixel events from an uncollimated ^{137}Cs source collected for 40 h from the whole volume of detector #2. The detector was biased at −1400 V on the cathode and −45 V on the anode grid.

An energy resolution of 1.23% FWHM at 662 keV has been achieved for two-pixel events collected from the entire volume of the second detector, as shown in Fig. 7. However, for three-pixel events the energy resolution degraded to 2.3% FWHM at 662 keV, as can be seen in Fig. 8.

When a 662 keV gamma ray interacts multiple times inside the detector volume, the probability of depositing all 662 keV energy is much higher than for only one interaction. Comparing Figs. 4(c), 7 and 8, the peak-to-Compton ratio increases from ∼11 for single-pixel events to ∼20 for two-pixel events and ∼35 for three-pixel events. The ability of sensing multiple interactions can be very useful in applications where the peak-to-total ratio determines the measurement sensitivity.

Due to the finite size of the electron cloud generated in the gamma-ray interaction, the number of interactions may not be equal to the number of pixels that collect electrons. This system does not have the ability to tell multiple interactions occurring under one pixel and one-interaction being shared by multiple pixels. In this paper, N-pixel events refer to those events in which N channels pass a pre-set noise threshold. The energy spectrum for two-pixel events in Fig. 7 clearly shows the Compton edge that is an indication of single Compton scattering interactions being shared by two pixels. The Compton edge faded away after we excluded all neighboring two-pixel events.

We also observed that the measured photopeak efficiency is lower in multiple-pixel events than the simulated results [14] by comparing the fraction of single-pixel (∼30%), two-pixel (∼40%) and three-pixel (∼20%) photopeak events. One major reason could be the fairly high triggering threshold of the current system—∼30 keV for the anode pixels and ∼50 keV for the cathode. The depth sensing for multiple-pixel events needs to measure the electron drift time for each individual pixel that passes the noise threshold. The cathode signal must pass the triggering threshold and each anode pixel that passes the noise threshold must also pass the triggering threshold. Therefore,

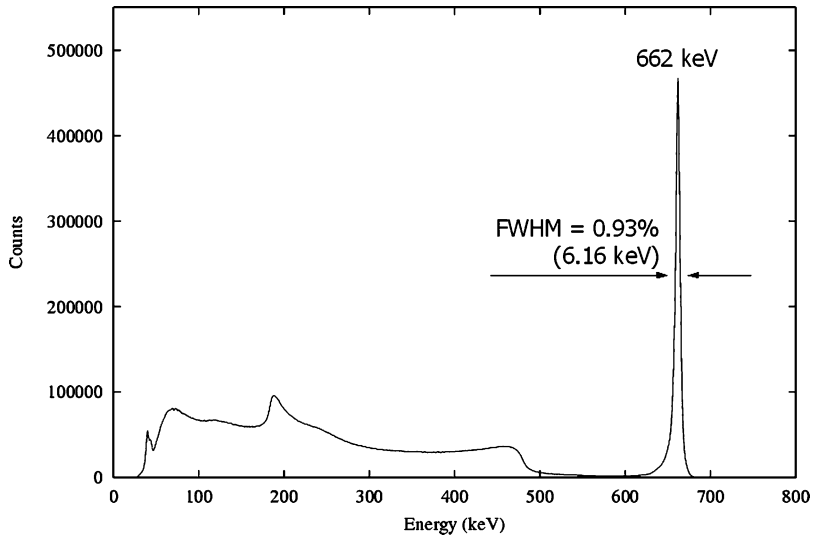

Fig. 9. Combined energy spectrum of all single-pixel, two-pixel and three-pixel events from an uncollimated ^{137}Cs source collected for 40 h from the whole volume of detector #2. The detector was biased at -2000 V on the cathode and -60 V on the anode grid.

some multiple-pixel events with one pixel having an energy deposition less than the triggering threshold have to be discarded.

The energy resolutions of 662 keV single-pixel and multiple-pixel events are summarized in Table I for the two detectors operated under different bias conditions. For single-pixel events, the first detector produced better results at higher cathode and grid biases, while the second detector achieved better resolutions at lower cathode and grid biases. This might be due to the much lower $(\mu\tau)_e$ of the first detector and thus the larger influence of the electron trapping on the energy resolution. Electronic noise was a dominant factor in the energy resolution for the second detector. Therefore, lower biases resulted in lower leakage current and lower electronic noise, and thus better energy resolution. For multiple-pixel events, both detectors achieved better energy resolution at higher biases, which might be due to better timing resolution and less charge sharing at higher biases.

The total energy spectrum of all single-pixel, two-pixel and three-pixel events collected from the second detector, which in theory should include nearly 90% of the 662 keV photopeak events that occurred inside the detector volume [14], is shown in Fig. 9. The detector was operated under -2000 V cathode bias and -60 V grid bias, irradiated by an uncollimated ^{137}Cs source from the cathode side for 40 h. An energy resolution of 0.93% FWHM at 662 keV was achieved. However, the observed photopeak efficiency is lower than expected mainly due to the fairly high triggering threshold as discussed previously.

TABLE I
ENERGY RESOLUTION (FWHM) AT 662 keV FOR SINGLE-PIXEL EVENTS AND MULTIPLE-PIXEL EVENTS FROM THE WHOLE BULK OF TWO SIMILAR DETECTORS

Detector	Single-Pixel Events	Two-Pixel Events	Three-Pixel Events
1 @ -1400 V, -45 V	0.95% (6.29 keV)	1.52% (10.06 keV)	2.67% (17.7 keV)
1 @ -2200 V, -65 V	0.93% (6.16 keV)	1.46% (9.67 keV)	2.41% (16.0 keV)
2 @ -1400 V, -45 V	0.76% (5.03 keV)	1.23% (8.14 keV)	2.33% (15.4 keV)
2 @ -2000 V, -60 V	0.78% (5.16 keV)	1.19% (7.88 keV)	2.08% (13.8 keV)

IV. DISCUSSION

Using the second detector as an example, an energy resolution of 0.76% FWHM at 662 keV was achieved for single-pixel events. But the energy resolution for two-pixel events was 1.23% FWHM, worse than the overestimated energy resolution based on two single-pixel events, a $\sqrt{(0.76\%)^2+(0.76\%)^2}=1.07\%$ FWHM. We analyze the factors affecting the energy resolution for two-pixel events in more detail below.

First, we have conservatively estimated the electronic noise to be $\sim$4.5 keV. The electronic noise from both pixels will contribute to the energy resolution degradation, at an estimated amplitude of $\sqrt{4.5^2+4.5^2}=6.4$ keV, assuming that the noises are not correlated.

Second, due to the timing resolution of 30 ns FWHM on the TAT3, the depth resolution for two-pixel events is $\sim$0.4 mm FWHM using the measured electron drift times. This uncertainty in the depth will contribute an uncertainty of 4% to the depth correction. Since the total change of the photopeak centroid across the whole thickness (1 cm) of the detector is $\sim$6%, this timing uncertainty contributes $4\% \times 6\% \times 662$ keV $=$ 1.59 keV.

Third, the depth resolution for single-pixel events is $\sim$0.2 mm FWHM and thus introduces a $\sim$% uncertainty in the depth correction, a $2\% \times 6\% \times 662$ keV $= 0.79$ keV. The contribution of factors other than electronic noise and depth uncertainty is $\sqrt{(0.76\% \times 662)^2-4.5^2-0.79^2}=2.1$ keV.

Then, by adding all these known factors, we can get an estimation of the energy resolution for two-pixel events—$\sqrt{6.4^2+1.59^2+2.1^2}=6.92$ keV FWHM or 1.05% FWHM. This is still smaller than the experimental

result of 1.23% FWHM. Other factors, accounting for $\sqrt{(1.23\% \times 662)^2 - 6.92^2} = 4.3$ keV FWHM are contributing to the energy resolution degradation for two-pixel events. Possible factors, such as charge sharing, poor depth resolution at low energy, and nonlinearity, are still under investigation.

Both detectors were fabricated by eV-Products more than three years ago and have been tested with both the VAS2/TAT2 readout system [7] and the VAS3.1/TAT3 readout system. There is no change in the detectors. Therefore, all improvements are due to the improvements in the readout electronics (the ASIC and the front-end board). The 3-D position sensitive CZT detectors should be able to achieve even better performance with CdZnTe crystals of higher $(\mu\tau)_e$ and better uniformity [15].

V. Summary

With the help of the third-generation ASIC-VAS3.1/TAT3, the performance of the 3-D position sensitive CZT spectrometer has been significantly improved. The electronic noise was reduced from 6 keV to less than 4.5 keV. The triggering thresholds of the anode pixels were lowered to ~30 keV. By implementing 3-D corrections, remarkable energy resolutions of 0.93% (6.16 keV) FWHM and 0.76% (5.03 keV) FWHM at 662 keV for single-pixel events have been achieved from the entire 2.25 cm^3 volumes. Energy resolutions for two-pixel events were 1.46% FWHM and 1.23% FWHM at 662 keV, worse than expected from statistical considerations. The reasons for the energy degradation in multiple-pixel events are still under investigation.

An energy resolution of 0.93% FWHM at 662 keV has been achieved for all single-pixel, two-pixel and three-pixel events collected from the second detector, which clearly demonstrates an improved spectroscopic capability of the 3-D position sensitive CZT spectrometers.

Acknowledgment

The authors would like to thank A. B. Young of the Radiation Oncology Department and B. E. Casey of the Electrical Engineering and Computer Science Department at the University of Michigan for their work on the wire-bonding during the assembly of these systems.

References

[1] P. N. Luke, "Unipolar charge sensing with coplanar electrodes-application to semiconductor detectors," *IEEE Trans. Nucl. Sci.*, vol. 42, no. 4, pp. 207–213, Aug. 1995.

[2] F. P. Doty *et al.*, "Pixelated CdZnTe detector arrays," *Nucl. Instrum. Meth. A*, vol. 353, pp. 356–360, 1994.

[3] Z. He, G. F. Knoll, D. K. Wehe, and J. Miyamoto, "Position-sensitive single carrier CdZnTe detectors," *Nucl. Instrum. Meth. Phys. Res. A*, vol. 388, pp. 180–185, 1997.

[4] Z. He, W. Li, G. F. Knoll, D. K. Wehe, J. E. Berry, and C. M. Stahle, "3-D position sensitive CdZnTe gamma-ray spectrometers," *Nucl. Instrum. Meth. Phys. Res. A*, vol. 422, pp. 173–178, 1999.

[5] W. Li, Z. He, G. F. Knoll, D. K. Wehe, and J. E. Berry, "A data acquisition and processing system for 3-D position sensitive CZT gamma-ray spectrometers," *IEEE Trans. Nucl. Sci.*, vol. 46, no. 6, pp. 1989–1994, Dec. 1999.

[6] Ideas ASA, Martin Linges vei 25, Snarøya, Norway.

[7] F. Zhang, Z. He, D. Xu, G. F. Knoll, D. K. Wehe, and J. E. Berry, "Improved resolution for 3-D position sensitive CdZnTe spectrometers," *IEEE Trans. Nucl. Sci.*, vol. 51, no. 5, pp. 2427–2431, Oct. 2004.

[8] C. E. Lehner, Z. He, and G. F. Knoll, "Intelligent gamma-ray spectroscopy using 3-D position-sensitive detectors," *IEEE Trans. Nucl. Sci.*, vol. 50, no. 4, pp. 1090–1097, Aug. 2003.

[9] C. E. Lehner, Z. He, and F. Zhang, "4π Compton imaging using a 3-D position-sensitive CdZnTe detector via weighted list-mode maximum likelihood," *IEEE Trans. Nucl. Sci.*, vol. 51, no. 4, pp. 1618–1624, Aug. 2004.

[10] eV-PRODUCTS, Saxonburg, PA.

[11] F. Zhang and Z. He, "3-D position sensitive CdZnTe gamma-ray spectrometers—improved performance with new ASICs," *Proc. SPIE*, vol. 5540, pp. 135–143.

[12] W. Li, Z. He, G. F. Knoll, D. K. Wehe, and C. M. Stahle, "Spatial variation of energy resolution in 3-D position sensitive CZT gamma-ray spectrometers," *IEEE Trans. Nucl. Sci.*, vol. 46, no. 3, pp. 187–192, Jun. 1999.

[13] Z. He, G. F. Knoll, and D. K. Wehe, "Direct measurement of product of the electron mobility and mean free drift time of CdZnTe semiconductors using position sensitive single polarity charge sensing detectors," *J. Appl. Phys.*, vol. 84, no. 10, p. 5566, 1998.

[14] Y. F. Du, W. Li, Z. He, G. F. Knoll, and D. K. Wehe, "Monte Carlo investigation of the charge sharing effects in 3-D position sensitive CdZnTe gamma ray spectrometers," *IEEE Trans. Nucl. Sci.*, vol. 46, no. 4, pp. 844–847, Aug. 1999.

[15] C. Szeles, S. E. Cameron, J. O. Ndap, and M. D. Reed, "Advances in the high-pressure crystal growth technology of semi-insulating CdZnTe for radiation detector applications," *Proc. SPIE*, vol. 5198, pp. 191–199, 2004.